On the formation of vase-shaped drops

Martin Coux, Pierre Chantelot, Lucie Domino, Christophe Clanet, Antonin Eddi, David Quéré

On the formation of vase-shaped drops

Martin Coux, Pierre Chantelot, Lucie Domino,
Christophe Clanet, Antonin Eddi & David Quéré

1. Physique et Mécanique des Milieux Hétérogènes, UMR 7636 du CNRS, ESPCI Paris, PSL Research University, 75005 Paris, France

2. LadHyX, UMR 7646 du CNRS, École polytechnique, 91128 Palaiseau, France

In most wetting situations, we try to understand how liquids spread or recoil when brought into contact with immobile substrates. The way drops at equilibrium react to the motion of the phase (either solid or liquid) on which they lie has been less studied, despite the variety of unexpected situations this generates, as can be illustrated by a few examples. If we first consider the case where the substrate is translated, an incoming liquid can be repelled by a viscous boundary of air, which generates its levitation [1-2]. Vibrating the underlying phase can lead to similar effects when it is liquid, which triggers not only the levitation of drops but also their propulsion on the waves at the bath surface [3-4]. The latter effect is not observed when vibrating a solid; instead, the deposited drop can itself vibrate radially, with star-like shapes when its contact line gets depinned [5-6]. These dynamics become especially spectacular when the substrate is inclined and the oscillation of large amplitude, which possibly leads to an uphill propulsion of the liquid, as reported in [7] and discussed in [8-11].

An extreme case of vibration is a kick, namely an impulsive rise and descent of the substrate. Such motions were used to fragment sessile drops [12] or to recover superhydrophobicity on textured materials, by depinning water from a Wenzel state to the much more frictionless Cassie state [13]. Impulsive motions can generate large accelerations, which was exploited to force liquids to spread in a reinforced gravity field [14], or conversely as a catapult to expel water from its substrate [15,16]. We discuss here how vertical kicks compel drops to successively spread, recoil and even takeoff – which happens, as we shall see, after developing unusual vase-like shapes that we describe and analyze.

Our experiment consists of subjecting a sessile, millimetric water drop to a kick. To that end, we fix an aluminum plate to a magnetic shaker (Bruel & Kjaer 4808) whose motion is controlled with an amplified hemi-sinusoidal signal with adjustable amplitude and frequency. In order to enhance the water mobility, we spray-coat aluminum with a commercial solution of hydrophobic nanobeads dispersed in acetone (Ultra Ever Dry, UltraTech International). After evaporation of the solvent, water exhibits the combination of high contact angles (~160°) and low hysteresis (~6°) characteristic of a superhydrophobic material. We adjust the horizontality of the substrate with a spirit level before depositing distilled water (density ρ = 1000 kg/m^3, viscosity η = 1 mPa.s and surface tension γ = 72 mN/m) under the form of drops with radius R_0 ranging from 1 mm to 1.8 mm, as provided by calibrated needles. The substrate motion $z(t)$, that is, the mechanical response of the shaker to the input signal, consists of a vertical rise by a distance varied between 5 mm and 10 mm within a time ranging from 3 ms to 10 ms followed

by a slower descent: the plate typically comes back to its initial position 20 ms after reaching its highest position. The maximal speed and acceleration of the substrate are thus on the order of 1-2 m/s and 50-100 g, respectively, denoting g as the acceleration of gravity. The drop deformations induced by the kick are recorded from the side with a high-speed video-camera (Phantom V7) at typically 10000 frames per second. We extract from the movies how the substrate moves with a sub-pixel accuracy, using standard correlation and interpolation algorithms [17] together with the evolution of the drop shape that we detect through an edge sensitive algorithm. The origin of time is defined when the displacement of the substrate reaches one pixel. We report in figure 1a (and in the corresponding video SI1) the successive states of a water droplet with initial radius $R_0 = 1.8$ mm subject to the kick displayed below the snapshots, that is, of height 7.5 mm and maximal speed $U = 1.90 \pm 0.07$ m/s reached at $\tau = 5.6 \pm 0.2$ ms.

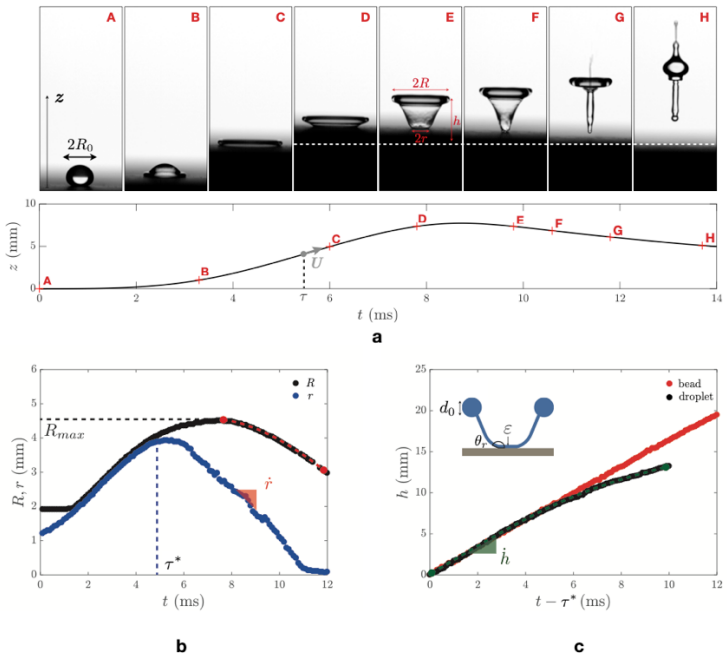

Figure 1. a. Water droplet with radius $R_0 = 1.8$ mm after a kick of its non-wetting substrate (top) and substrate position (bottom). The plate rises until reaching its maximum speed $U = 1.90 \pm 0.07$ m/s at time $\tau = 5.6 \pm 0.2$ ms. Letters refer to corresponding pictures. The droplet is strongly reshaped and forms a liquid vase, with a toroidal rim of maximal extension $2R(t)$, at height $h(t)$ above the takeoff altitude $z(\tau^*)$ (indicated by the white dashed line), and a circular liquid-solid contact of diameter $2r(t)$. **b**. Time evolution of the radii $R(t)$ (black data) and $r(t)$ (blue data) for a droplet ($R_0 = 1.8$ mm) subject to a kick with $U = 1.50 \pm 0.03$ m/s and $\tau = 3.4 \pm 0.2$ ms. The rim takes off at time $\tau^* = 4.8 \pm 0.3$ ms after which $r(t)$ linearly decreases with time with speed $|\dot{r}| = 0.80 \pm 0.05$ m/s. $R(t)$ increases until its maximal extension R_{max} and then it decreases at constant acceleration $\ddot{R} = 72 \pm 2$ m/s^2 (red dashes). **c**. Time evolution of the altitude of the peripheric rim for a drop with $R_0 = 1.8$ mm (black data) and for a propylene bead with similar size ($R_0 = 1.75$ mm) and density ($\rho = 950$ kg/m^3) (red data) for a kick with $U = 1.70 \pm 0.02$ m/s and $\tau = 4.9 \pm 0.2$ ms. Both objects take off at the same time τ^*, with the same velocity $\dot{h} = 1.8 \pm 0.1$ m/s. Dashes show a parabolic fit of the rim trajectory, $h(t) = \dot{h}t - \ddot{h}t^2/2$, with $\ddot{h} = 97 \pm 6$ m/s^2. Inset: Sketch of a liquid vase, the rim has a minor diameter d_0. The liquid-solid contact is a disk with thickness ε that meets the solid at an angle θ_r.

The kick dramatically reconfigurates the liquid: the drop first spreads as the substrate rises (A-C) with a shape reminiscent of an impacting drop; then ($t > 7.2$ ms), the peripheric rim takes off and the inner film remains in contact with the substrate, as shown in D. As it rises, the upper rim keeps a nearly constant diameter while the film recoils, which leads to the formation of a vase-shaped cavity (pictures E to F, around $t \approx 10$ ms). This cavity eventually collapses and takes off (point G), which triggers the eruption of a jet (starting in G and more developed in H) rising at a velocity on the order of 10 m/s and comparable to those described in the context of strong droplet impact [18] and bubble collapse [19].

At the short timescales of the experiment, we expect inertia to be the dominant resistance to motion, which qualitatively explains the formation and evolution of a shape resulting from the redistribution of mass induced by the kick. Indeed, vase shapes evidence that the liquid still in the vicinity of the solid is thin (and thus mobile), while the torus formed at the periphery after spreading carries most of the liquid mass, and thus transiently appears as more static. This observation is made quantitative by plotting the two distances r and R that define the water vase; r is the water/solid contact radius, while R is the maximum water radius and thus the radius of the vase top rim once it has formed, as sketched in figure 1a, instant E. R and r are recorded until jetting, the moment when the vase disappears. We show an example of the evolution of these two radii in figure 1b, for a drop with $R_0 = 1.8$ mm subject to a kick with $U = 1.50 \pm 0.03$ m/s and $\tau = 3.4 \pm 0.2$ ms. During spreading, both radii increase the same way ($R = r$) as soon as we have $r > R_0$; these two distances separate at a time τ^*, when the rim takes off. We determine τ^* with a precision of less than 0.5 ms by detecting the presence of light below the rim, the experiment being backlit. Later, r and R behave independently: on the one hand, the contact radius r decreases linearly with time, from which we deduce a dewetting velocity $|\dot{r}| \approx 0.80 \pm 0.05$ m/s; on the other hand, the torus keeps expanding because of inertia, until it reaches its maximal extension R_{max}. Later, instead of retracting at a constant velocity, and as shown by the parabolic fit with red dashes in figure 1b, the torus collapses with a constant acceleration $|\ddot{R}| = 72 \pm 2$ m/s^2.

The description of the water vase can be completed by a discussion on its height. As sketched in figure 1a, we denote this quantity as h, considered in the reference frame of the lab and set to 0 at the takeoff of the rim ($h(\tau^*) = 0$). We also define and represent in the insert of figure 1c other characteristics of the vase, such as the inner diameter d_0 of its rim, the mean thickness ε

of its base, and the receding angle of water, θ_r. We observe that θ_r keeps a constant value during the dewetting stage despite the change in angle between the substrate and the cavity wall. From independent tilt measurements, we obtain $\theta_r = 155 \pm 2°$. In figure 1c itself, we plot the vase height h as a function of time after takeoff at $t = \tau^*$ for a drop whose substrate rises at maximal velocity $U = 1.70 \pm 0.02$ m/s reached at time $\tau = 4.5 \pm 0.2$ ms. The height h of the vase first increases linearly with time (ballistic motion), at a velocity $\dot{h} \approx 1.8 \pm 0.1$ m/s $\approx U$ – as does the solid bead. However, the vase rise slows down, and fitting the trajectory by a parabola ($h(t) = \dot{h}t - \ddot{h}t^2/2$, dashes in the figure) provides a deceleration $\ddot{h} = 97 \pm 6$ m/s^2 much larger than gravity, whose effect is indeed invisible for the bead.

Hence kicked water drops adopt the unique shape of truncated cones, which we now model. The first step of the drop transformation is found to be quite usual, resembling to what is seen after an impact. Multiple scaling laws have been proposed to describe the maximum spreading radius of spreading drops [14,20]. For water impacting superhydrophobic substrates, a force balance yields $R_{max} \sim R_0\ We^{1/4}$. In figure 2a, we find that the maximum radius R_{max} of the transient puddle follows a power law in Weber number $We = \rho U^2 R_0/\gamma$. The exponent is indeed 0.25 ± 0.03 and the prefactor is 0.93 ± 0.10.

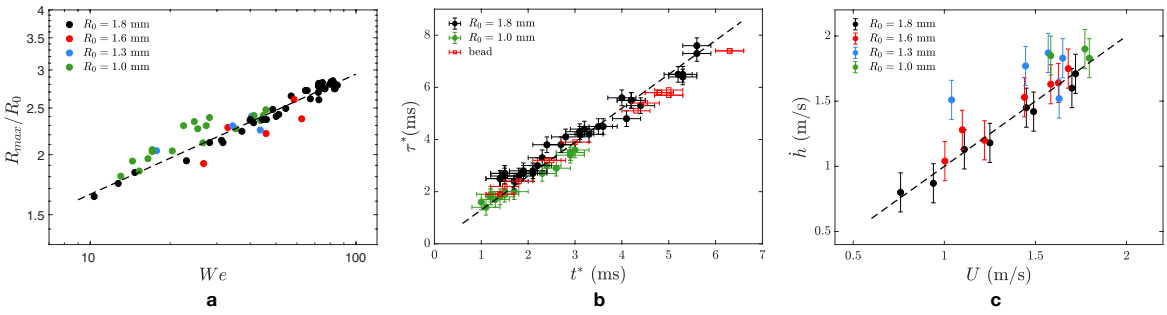

Figure 2. a. Spreading parameter R_{max}/R_0 of the drop as a function of the Weber number $We = \rho U^2 R_0/\gamma$, for drops of various radii R_0. Dashes show a power law of exponent 0.25 ± 0.03 and prefactor 0.93 ± 0.1. **b**. Takeoff time τ^* as a function of the time t^* such that $\ddot{z}(t^*) = -g$. Data for drops ($R_0 = 1$ mm and $R_0 = 1.8$ mm) and for polypropylene beads collapse on a line of slope 1.3. **c**. Takeoff speed $\dot{h}$ as a function of the maximal kick velocity U for four drop radii R_0. The dotted line has a slope 1.

Water vases form after this spreading phase, as the plate decelerates – a phenomenon which is not at stake in an impact. More precisely, the rim takes off at $t = \tau^*$, with a motion similar to that of a solid bead (figure 1c), which suggests an inertial mechanism: we expect the liquid to

take off at a velocity U when the plate acceleration reaches the value $-g$. This happens at a time t^*, which we deduce from a second order Savitzky-Golay fit of the function $z(t)$ in a window of 2 ms [21]. Smoothing improves the precision of the derivation steps and allows us to measure the acceleration $\ddot{z}(t)$ with a higher reproducibility. In figure 2b, we compare the time t^* with τ^* for two drops (R_0 = 1 mm and R_0 = 1.8 mm) and for one non-deformable drop, that is a polypropylene bead with similar size and density, all undergoing different kicks. τ^* and t^* are observed to be proportional to each other, as shown by the dashed line of slope 1.3 ± 0.15. The inertial behavior is confirmed by plotting the takeoff speed $\dot{h}(\tau^*)$ as a function of the maximal velocity U of the substrate. As seen in figure 2c, the two velocities are similar, which we highlight with a dashed line of slope 1. We attribute the delayed takeoff of the drops and the bead to an experimental artifact: the substrate and the lens's axis are not strictly parallel leading to an overestimation of τ^*.

However, the drop does not takeoff at once. At $t > \tau^*$, a liquid film with thickness ε located inside the rim still contacts the plate from which it dewets at a constant velocity $\dot{r}$ on the order of 1 m/s. The corresponding Reynolds number $Re = \rho\dot{r}\varepsilon/\eta$ is typically 100, which suggests an inertial dewetting, as first described by Taylor and Culick for suspended films [22-23] and later by Buguin *et al.* for water films on non-wetting substrates [24]. In our experiments, the thin dewetting film does not feed a rim but a system composed of the free-standing film and the toroidal rim. We assume the variation of horizontal momentum of this system comes, at first order, from the liquid feeding it, the horizontal dynamics of the free-standing film and the torus being slow compared to the dewetting process. The thin-film dynamics is then expected to result from the balance of lineic momentum rate $\rho\dot{r}^2\varepsilon$ with lineic surface forces $\gamma(1 - \cos\theta_r)$, so that we can deduce the (unknown) film thickness ε from the dewetting speed $\dot{r}$. Retraction takes place at velocities varying from 0.45 m/s to 1.15 m/s, which yields film thicknesses in the range of tens to hundreds of micrometers (for θ_r = 155°), in good qualitative agreement with values known at impact [25-26]. The film volume $\omega \approx \pi R_{max}^2\varepsilon$ can finally be compared to the drop volume $\Omega = 4\pi R_0^3/3$. For typical values (R_0 = 1.8 mm, R_{max} = 4.5 mm, ε = 140 μm), we find a ratio $\omega/\Omega \approx 0.35$, which confirms that liquid is mainly concentrated in the top rim.

This preliminary description provides the initial shape of the vase: the rim rises at a velocity $\dot{h}$ comparable to the dewetting speed $\dot{r}$ of the film, and these independent motions lead to a conical cavity of aperture angle around 45° – as observed in figure 1a. However, the vase

transformations are not homothetic, owing to the contrast of dynamics between the film and the rim. As we saw, rims take off at a velocity $\dot{h} \approx U$ and slow down with a constant deceleration $\ddot{h}$ equal to a few tens of g (figure 1c). In the meantime, it shrinks from its initial radius R_{max} with a constant acceleration $\ddot{R}$ comparable to $\ddot{h}$. We assume that these two dynamics result from a balance of inertia with a constant force, since the limited exchanges of matter between the film and the rim allow us to treat the rim mass M as constant all along the motion. For the sake of simplicity, we scale this mass by the drop mass $\rho\Omega$ and express its constant value by volume conservation $\Omega \approx R_0^3 \approx R_{max}\, d_0^2$. 1) Along the vertical direction, four forces apply to the liquid torus: (i) the vertical component of the traction $F_\gamma = 4\pi R\gamma$ exerted by the water film on the torus perimeter, typically of a few mN; (ii) gravity Mg, typically 100 µN; (iii) aerodynamic drag $\rho_{air}\dot{h}^2\pi R_{max}^2$ [27], that is, a few µN; (iv) the suction force arising from air being entrained under the rim as it takes off, which we neglect after noticing that the walls of the cavity always form an angle with the substrate large enough to prevent the formation of a lubrication air film. The capillary force F_γ is thus expected to be the dominant force in the vertical direction. We evaluate it at the onset of closure ($R \approx R_{max}$), which provides an upper bound for F_γ. The projection of Newton's law on the vertical axis yields: $\rho R_0^3 \ddot{h} \sim \gamma R_{max}$, *i.e.* $\ddot{h} \sim \gamma R_{max}/\rho R_0^3$. 2) Along the horizontal direction, two forces tend to close the rim, namely the horizontal component of F_γ and the force $F_\gamma' \sim 2\gamma R_0^3/R_{max}d_0$ generated by the difference of Laplace pressure between the inner and outer sides of the torus [28]. The ratio F_γ/F_γ' scales as R_{max}/d_0, a quantity typically of order 10 as seen with high angle views of the kicked droplets (insert in figure 3b and video SI2 in the Supplementary Information). Hence, we assume that F_γ (also) dominates in the horizontal direction, from which we deduce from the force balance $\rho R_0^3 \ddot{R} \sim \gamma R_{max}$ a constant acceleration $\ddot{R} \sim \gamma R_{max}/\rho R_0^3 \sim \ddot{h}$ for the rim closure.

As observed in figures 1b and 1c, both accelerations $\ddot{h}$ and $\ddot{R}$ can be deduced from parabolic fits of the rim position. In figures 3a and 3b, we compare these measurements with the values expected from our model. In the whole range of parameters (varied by a factor 4 by modifying the characteristics of the kick and the drop volume), we find a linear relationship between the two quantities, with a slope equal to 2.1 ± 0.3 for $\ddot{h}$ and 2.1 ± 0.2 for $\ddot{R}$. The agreement can be considered as satisfactory, considering the simplicity of the model. We can also note that error bars are larger in figure 3a, due to the high sensitivity to the selection of the start and end points of the fit of $h(t)$ and to the adjustment of two parameters, namely $\dot{h}$ and $\ddot{h}$.

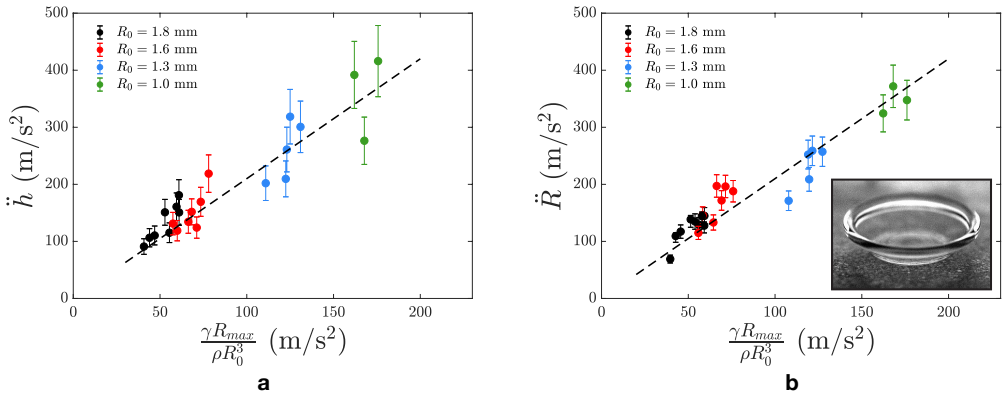

Figure 3. a and **b**: Deceleration $\ddot{h}$ of the rim height and acceleration $\ddot{R}$ of its closure as a function of the quantity $\gamma R_{max}/\rho R_0^3$ derived by balancing the rim inertia with surface tension. Dashed lines are linear fits of slope 2.1 ± 0.3 and 2.1 ± 0.2 respectively. Inset in **b**: high-angle shot of a typical vase, which provides the ratio $2R_{max}/d_0$ (7, here).

These considerations allow us to discuss how liquid vases are sculpted by the interplay between the respective dynamics of the rim and of the film. At takeoff, $h(t)$ and $r(t)$ both vary linearly with time, while the rim radius R remains roughly constant ($R \approx R_{max}$), leading to the creation of conical cavities. Kicks generate both the rim and its takeoff, so that the vase shape can be tuned by playing on the solid/liquid pining that sets the dewetting velocity of the film. To check this hypothesis, we performed a series of five experiments at given kick ($U = 1.70 \pm 0.02$ m/s, $\tau = 4.9 \pm 0.2$ ms) and drop size ($R_0 = 1.8$ mm), yet on different substrates. The three first trials were performed on less and less sticky materials, with respective receding angle $\theta_r = 85 \pm 3°$ (glass slide made hydrophobic with trichloroperfluoro-octylsilane), $\theta_r = 145 \pm 3°$ (repellent substrate made by photolithography), and $\theta_r = 155 \pm 2°$ (super-hydrophobic substrate coated by hydrophobic nanobeads, cf supra). The spreading phase is comparable in the three cases, and shapes are compared 3.0 ± 0.2 ms after the rim takeoff. As it can be seen in figures 4a, 4b and 4c and in corresponding videos SI3 and 4, the resulting vases are quite different. Firstly, the angle between the vase sides and horizontal decreases from ~100° to ~65°, so that we pass from a quasi-cylinder to a quasi-cone, consistently with our model: as the receding contact angle increases, the dewetting velocity of the water film increases, so that the base of the vase becomes more and more narrow. Secondly, reshaping induces changes of the projection of the force applied by the film on the rim, so that the height and radius of the rim slightly increase and decrease, respectively, at larger θ_r.

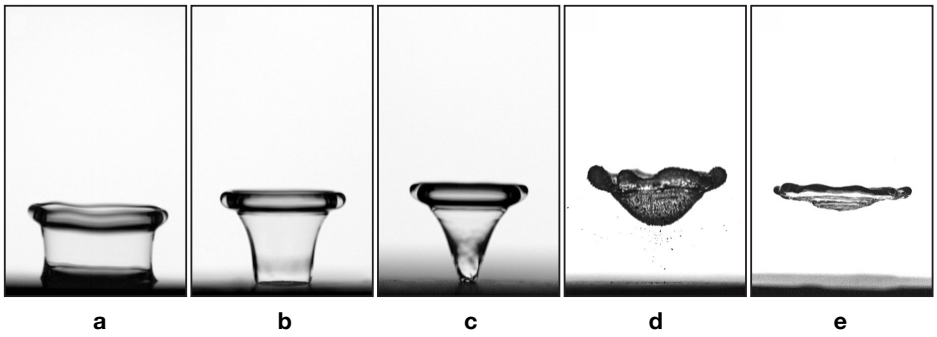

Figure 4. Shape of water drops (R_0 = 1.8 mm) 3 ± 0.2 ms after a kick with U = 1.7 ± 0.1 m/s and τ = 4.9 ± 0.2 ms, for different wetting conditions. **a.** On silanized glass, the receding angle of water (which characterizes pinning on the substrate) is 85 ± 3°. **b.** On a substrate covered with micrometric, hydrophobic pillars, it is 145 ± 3°. **c.** On a substrate with hydrophobic nanobeads, it is 155 ± 2°. The vase shape gradually evolves from a cylinder to a cone. **d.** For a non-wetting liquid marble (water covered with hydrophobic beads) or **e.** for a Leidenfrost drop, the vase becomes a bowl or even a plate.

Hydrophobicity can be made even more extreme. Firstly, we coat the water drop with silanized lycopodium grains (diameter of 30 μm) and deposit the resulting liquid marble on a non-wetting plate. The solid/liquid contact is thus minimized by the presence of the micrometric particles [29]. Secondly, we consider a 50/50 mixture of water and ethanol placed on a curved plate brought to a temperature of 300°C. The resulting Leidenfrost state presents strictly no adhesion, since the liquid then floats above a cushion of its own vapor [30]. These two drops are subject to the same kick as previously, and their shapes after takeoff are presented in figures 4d and 4e (the full events can be seen in videos SI5 and 6). While the spreading stage is similar to the previous cases, no liquid remains in contact with the plate after the rim takes off, which impedes the generation of a cavity. The suppression of pinning between the liquid and the plate rather leads to the global takeoff of the pancake obtained after spreading. Interestingly, the liquid marble (figure 4d) adopts a curved shape whereas the Leidenfrost droplet is completely flat (figure 4e). More precisely, coated drops take off flat and get curved only a few instants later; this suggests that the air penetrating underneath is responsible for the curvature of the flattened liquid, as does the movement of lycopodium grains in air (see Supplementary movie SI5). This suction effect is not observed for the Leidenfrost droplet, which might be due to the differences between the two systems: in the Leidenfrost regime, (i) liquid and solid are separated by a vapor cushion whose thickness is on the order of 100 μm; (ii) there is a radial vapor flow under the droplet going from inside to outside, countering the suction. Apart from these small differences, these final experiments emphasize that the presence of a contact line is a necessary condition for generating vases, even at low contact angle hysteresis.

In summary, we described and modeled how droplets deposited on a superhydrophobic substrate are strongly reshaped after a kick. The coexistence of fast and slow dynamics leads to the apparition of beautiful and unusual conical cavities. Understanding the different physical processes at stake allowed us to tune the shape of the vases by playing on the wetting properties of the substrate and to evidence the role of adhesion. We restricted our analysis to the creation and evolution of the cavities. Their collapse would also deserve a separate study as they lead to the creation of fast jets. In addition, the high-speed motion of a superhydrophobic substrate might enhance its water-repellent properties, which should be explored by coupling droplet impacts with impulsive motions.

References

[1] O.A. Povarov, O.I. Nazarov, L.A. Ignat'evskaya and A.I. Nikol'skii, « Interaction of drops with boundary layer on rotating surface », Journal of Engineering Physics **31**, 1453-1456 (1976).
[2] K.R. Sreenivas, P.K. De and J.H. Arakeri, « Levitation of a drop over a film flow », Journal of Fluid Mechanics **380**, 297-307 (1999).
[3] Y. Couder, E. Fort, A. Boudaoud and C.H. Gautier, « From bouncing to floating: Noncoalescence of drops on a fluid bath », Physical Review Letters **94**, 177801 (2005).
[4] Y. Couder, S. Protière, E. Fort and A. Boudaoud, « Dynamical phenomena: Walking and orbiting droplets », Nature **437**, 208-208 (2005).
[5] X. Noblin, A. Buguin and F. Brochard-Wyart, « Vibrated sessile drops: Transition between pinned and mobile contact line oscillations », The European Physical Journal E **14**, 395-404 (2004).
[6] E. De Jong, Y. Wang, J.M.J. Den Toonder and P.R. Onck, « Climbing droplets driven by mechanowetting on transverse waves », Science Advances **5,** eaaw0914 (2019).
[7] P. Brunet, J. Eggers and R.D. Deegan, « Vibration-induced climbing of drops », Physical Review Letters **99**, 144501 (2007).
[8] X. Noblin, R. Kofman and F. Celestini, « Ratchetlike motion of a shaken drop », Physical Review Letters **102**, 194504 (2009).
[9] N. Savva and S. Kalliadasis, « Low-frequency vibrations of two-dimensional droplets on heterogeneous substrates », Journal of Fluid Mechanics **754,** 515-549 (2014).
[10] H. Ding, X. Zhu, P. Gao and X.-Y. Lu, « Ratchet mechanism of drops climbing a vibrated oblique plate », Journal of Fluid Mechanics **835,** R1 (2018).
[11] T. Bradshaw and J. Billingham, « Thick drops climbing on an oscillating substrate », Journal of Fluid Mechanics **840,** 131-153 (2018).
[12] Y.-S. Shin and H-C. Lim, « Shape oscillation and detachment conditions for a droplet on a vibrating flat surface », The European Physical Journal E **37**, 74 (2014).
[13] J.B. Boreyko and C.-H. Chen, « Self-propelled dropwise condensate on superhydrophobic surfaces », Physical Review Letters **103**, 174502 (2009).
[14] C. Clanet, C. Béguin, D. Richard and D. Quéré, « Maximal deformation of an impacting drop », Journal of Fluid Mechanics **517**, 199-208 (2004).
[15] C. Raufaste, G.R. Chagas, T. Darmanin, C. Claudet, F. Guittard and F. Celestini, « Superpropulsion of droplets and soft elastic solids », Physical Review Letters **119**, 108001 (2017).
[16] W. Wang, C. Ji, F. Lin, J. Zou and S. Dorbolo, « Water drops bouncing off vertically vibrating textured surfaces », Journal of Fluid Mechanics, **876**, 1041-1051 (2019).
[17] A. Marchand, « Mouillage statique et dynamique : Influences géométriques aux échelles *moléculaires* », PhD thesis, Université Paris Diderot (2011).

[18] D. Bartolo, C. Josserand and D. Bonn, « Singular jets and bubbles in drop impact », Physical Review Letters **96**, 124501 (2006).
[19] L. Duchemin, S. Popinet, C. Josserand and S. Zaleski, « Jet formation in bubbles bursting at a free surface », Physics of Fluids **14**, 3000-3008 (2002).
[20] N. Laan, K.G. de Bruin, D. Bartolo, C. Josserand and D. Bonn, « Maximum diameter of impacting liquid droplets », Physical Review Applied **2,** 044018 (2014).
[21] A. Savitzky and M.J. Golay, « Smoothing and differentiation of data by simplified least squares procedures », Analytical Chemistry **36**, 1627-1639 (1964).
[22] G.I. Taylor, « Fluid flow in regions bounded by porous surfaces », Proc. R. Soc. London, Ser. A **234**, 456-475 (1956).
[23] F.E.C. Culick, « Comments on a ruptured soap film », Journal of Applied Physics **31**, 1128-1129 (1960).
[24] A. Buguin, L. Vovelle and F. Brochard-Wyart, « Shocks in inertial dewetting », Physical Review Letters **83**, 1183-1186 (1999).
[25] G. Lagubeau, M.A. Fontelos, C. Josserand, A. Maurel, V. Pagneux and P. Petitjeans, « Spreading dynamics of drop impacts », Journal of Fluid Mechanics **713**, 50-60 (2012).
[26] H. Lastakowski, F. Boyer, A.L. Biance, C. Pirat and C. Ybert, « Bridging local to global dynamics of drop impact onto solid substrates », Journal of Fluid Mechanics **747**, 103-118 (2014).
[27] The Reynolds number $\rho_{air} R_{max} \dot{h}/\eta_{air}$ associated to the flow around the rising torus is on the order of 1000, so that the drag force is taken $\propto \dot{h}^2$.
[28] B. Darbois-Texier, K. Piroird, D. Quéré and C. Clanet, « Inertial collapse of liquid rings », Journal of Fluid Mechanics **717**, R3 (2013).
[29] P. Aussillous and D. Quéré, « Liquid marbles », Nature **411**, 924-927 (2001).
[30] J.C. Burton, A.L. Sharpe, R.C. van der Veen, A. Franco, and S.R. Nagel, « Geometry of the vapor layer under a Leidenfrost drop », Physical Review Letters **109**, 074301 (2012).